LPC CAEN

LABORATOIRE DE PHYSIQUE CORPUSCULAIRE

ISMRA - Boulevard Maréchal Juin - 14050 CAEN CEDEX - FRANCE

THE PHOSWICH DETECTOR ARRAY OF THE FORWARD RING OF INDRA

J.C. Steckmeyer, D. Cussol, J. Duchon, J.M. Gautier, J.L. Laville, P. Le Botlan, A. Leconte, J. Lelandais, V. Métivier, P. Mosrin, E. Rosato, J. Tillier, A. Wieloch

November 1994 **LPCC 94-13**

Submitted to Nuclear Instruments and Methods in Physics Research

INSTITUT NATIONAL
DE PHYSIQUE NUCLEAIRE ET DE PHYSIQUE DES PARTICULES

CENTRE NATIONAL DE LA RECHERCHE SCIENTIFIQUE

INSTITUT DES SCIENCES
DE LA MATIERE ET DU RAYONNEMENT

UNIVERSITÉ DE CAEN

Téléphone : 31 45 25 00
Télécopie : 31 45 25 49

THE PHOSWICH DETECTOR ARRAY OF THE FORWARD RING OF INDRA

J.C. Steckmeyer, D. Cussol, J. Duchon, J.M. Gautier, J.L. Laville [1], P. Le Botlan, A. Leconte, J. Lelandais, V. Métivier, P. Mosrin, E. Rosato [2], J. Tillier and A. Wieloch [3]

Laboratoire de Physique Corpusculaire, ISMRA, IN2P3-CNRS et Université de Caen 14050 Caen Cédex, France.

Abstract : The most forward ring ($2 \leq \theta \leq 3°$) of the INDRA multidetector has been equipped with 12 plastic phoswich detectors able to withstand the high counting rates encountered at very small angles. Each phoswich detector is composed of a 500 μm thick fast scintillator and a 25 cm thick slow scintillator. Elemental identification is achieved on a fairly large domain, ranging from Z = 1 up to Z = 37. A new method of Z separation, using an identification function technique, is described.

Permanent address :

1- SUBATECH, 44072 Nantes Cédex 03, France

2- Dipartimento di Scienze Fisiche, Universita di Napoli, 80125 Napoli, Italy

3- Institute of Physics, Jagellonian University, Reymonta 4, 30059 Krakow, Poland

1. Introduction

The INDRA multidetector consists of 336 detection cells arranged in 17 concentric rings coaxial about the beam axis (see fig. 1 and ref. 1). It is mainly devoted to detect particles and fragments emitted in high multiplicity events. The typical detection cell is a two or three element telescope made up of an ionization chamber, a silicon detector (up to $\theta = 45°$) and a CsI (Tl) scintillator, except for the forward ring which has been equipped with phoswich detectors. The phoswiches consist of a combination of NE102 and NE115 plastic scintillators. To conform with the general design of INDRA, this phoswich ring is composed of 12 modules, covering the polar angular range of 2° - 3°.

The use of phoswich detectors has been guided by the following considerations :

1) At the GANIL energies, in the forward direction, one deals with high counting rates since the grazing angles are very small for most of the systems. Then, plastic scintillators as NE102 and NE115 with decay time constant of 2.4 and 320 ns, respectively [2-3], are well suited in that case because of their fast response.

2) Plastic scintillators are easy to machine in various shapes and sizes. Thus, they permitted to satisfy the constraining mechanical design of the INDRA geometry. Furthermore, the possibility of building very close-packed arrays minimizes the dead areas ensuring a full geometrical efficiency.

3) Plastic scintillators are available with large thicknesses, allowing the detection of energetic light charged particles. This is done at a low cost compared with other detectors, as solid-state detectors, for which the cost is much higher if both detectors and electronics are taken into account.

Drawbacks of plastic scintillators are the non linearity of the light response to the energy deposit, as well as a rather weak intrinsic energy resolution. Furthermore, the phoswich technique imposes high identification thresholds for medium heavy ions. However, in the energy domain where INDRA is planned to operate (more than ~ 30 MeV/nucleon), this limitation is not really a problem, especially in the forward direction, where the interaction is dominated by the fast elastic and quasi-elastic components. Evidently, this threshold limit depends on the ΔE thickness.

Large arrays of plastic phoswiches have already been used in the intermediate energy domain ($E < 100$ MeV/nucleon) [4-10] as well as in the relativistic energy domain [11]. The authors of ref. [4] used an array of plastic phoswiches for the identification of $Z = 1$ and $Z = 2$ particles produced in heavy ion induced fusion reaction at low bombarding energy. A fast plastic with a thickness as low as 0.1 mm was used. Large forward hodoscope arrays have also been dedicated for measuring light particles and fragments emitted in the forward hemisphere [5-8]. An isotopic separation of H nuclei as well as an identification of fragments up to $Z \sim 10$

were achieved using fast plastic scintillators with a thickness lower than or equal to 1 mm [5-7]. An even better identification was obtained using lower photomultiplier tube (PMT) gains (and losing the Z = 1 particles below the threshold) ; an elemental resolution from Z = 2 through Z = 23 was performed [6]. Using thicker fast scintillator improves the separation of light charged particles and nuclei. For this purpose, thicknesses of ~ 1.6 and 3.2 mm were employed in the MSU 4π array [9], while the MEDEA multidetector is equipped with 2 mm thick fast scintillators [10]. At last more thicker layers are needed for the detection of pions, protons, deuterons and tritons produced in relativistic heavy ion collisions [11].

Since one of the main goals of INDRA is to identify element by element up to Z=40, it is necessary to obtain with the phoswiches a Z identification up to relatively large values. This imposes to cope with low thicknesses of the fast scintillator, less than 1 mm, in order to deal with reasonable thresholds for the identification of fragments.

The purpose of this paper is to present how the phoswich technique can be extended to the identification of high Z values ($1 \leq Z \leq 40$). Section 2 describes the various tests made to optimize the characteristics of the INDRA phoswich ring. Section 3 presents the electronics specifically designed for the phoswhich detectors. In section 4 is explained the method used to obtain element identification and separation. Section 5 deals with the energy calibration procedure.

2. Design of the detector

2.1. Study of geometrical definition

Various thicknesses of the fast plastic scintillator have been tested : 50 μm, 115 μm, 200 μm, 370 μm and 500 μm. Low thicknesses permit lower energy thresholds and elemental Z identification over a larger energy range. However, one is faced with the problem of finding the best compromise between conflicting requirements : low energy thresholds and a high Z identification against good separation of fragments and efficiency for light charged particles. Tests have been performed using a 35 MeV/nucleon Ca beam at the SARA facility at Grenoble and then with beams of Kr at 60 MeV/nucleon and Xe at 44 MeV/nucleon at GANIL. According to the specific geometry we chose, the thickness of 500 μm was the best compromise, the lower thicknesses leading to a poor Z resolution. As seen later, identification of fragments is achieved up to Z = 37. However, with such a thickness, the isotopic separation of H nuclei is no longer possible.

The length of the slow plastic scintillator should allow the detection of protons up to 200 MeV of energy. This implies a length of 25 cm. The required geometry (a ring of 12 modules at $2° \leq \theta \leq 3°$) leads to a small front area (~ 6.25 cm^2). Thus, the possibility of particle cross-talk from adjacent detectors due to multiple scattering has to be considered. Simulations

using the GEANT code [12] were done for lengths of 15 and 25 cm crossed by protons, deuterons and tritons. Various shapes of the simulated energy spectra have been tested, from a steep exponential slope up to the extreme case of a flat spectrum. They showed that the fraction of lost particles due to cross-talk was nearly the same in the 25 cm thickness case as in the 15 cm one. Moreover a longer slow scintillator was shown to improve the resolution of the high energy part of the H isotopes. The rate of particles escaping from one module is less than 1.3 %. This allowed us to decide for a length of 25 cm.

2.2. The photomultiplier bases

To avoid noise pick-up and simplify cabling of the electronics attached to each type of detector in INDRA it was decided to locate the low level analog circuits very close to every detector. This applies to the dividers feeding the 324 PMT's attached to the CsI(Tl) scintillators and the 12 ones attached to the phoswiches. These 336 dividers would dissipate a prohibitive amount of heat if using standard resistive chains. The amount of heat tolerated must be kept to a minimum to avoid drift of the PMT gain and of the parameters of the scintillators, not to mention the dividers themselves. With this in mind it appeared that a special design of dividers, using Field Effect Transistors (FET) to reduce power consumption, should be undertaken. This study was made at IPN Orsay for the CsI(Tl) PMT's [13]. It was then adapted to the XP2982 PMT's used with the phoswiches ; taking care of the high peak currents generated by heavy fragments stopped in the detector, plus the high average divider currents involved in case of high counting rates. A reduction factor of 100 in the power dissipated was thus attained with comparison to standard resistive chains.

Tests with pulsed light from fast Light Emitting Diode (LED) lamps and laser stimulated scintillators showed that the bases could largely withstand the peak and average currents anticipated with the phoswiches in the worst cases. Further checks on the completed detector with heavy-ion beams validated the behaviour of the array.

As mentioned in Sect. 1, plastic scintillators can cope with the high counting rates encountered at low angles. We have checked the gain stability of every detector against increasing beam intensities. The response remains stable up to 12 000 particles/s. This limit is considered safe for the experimental situations since, due to the other restricting factors (current in the CsI(Tl) PMT chains, dead time in data acquisition, random coincidences), the counting rate endeavoured by the phoswiches will not exceed 2 000 particles/s.

2.3. Final configuration

The phoswich ring integrated in the INDRA ensemble is shown in fig. 2. It is composed of 12 modules, each module comprising a 500 μm thick NE102 scintillator and a 25 cm thick NE115 scintillator with the fast scintillator glued with optical cement to the slow

scintillator. These two scintillators are followed by a 29 mm diameter XP2982 PMT directly glued to the back face of the NE115. They detect reaction products emitted in the 2° - 3° polar angle range with 360° of azimuthal acceptance (30° per module). The front window of the fast scintillator is at a distance of 130 cm from the target. The solid angle of each detector is 0.37 msr. The geometrical ring structure chosen for INDRA imposes tapered scintillators with trapezoidal shapes for the entrance and exit faces, the area of the latter being larger than the former one. This overall ring geometry allows the particles to cross very similar lengths inside each detector module and heretofore the lost energies are identical for the same nuclei carrying the same energy.

A 17 μm thick aluminum foil is sticked on the front face of the fast scintillator in order to eliminate the spurious contribution of soft electrons and also to improve the light reflection inside the scintillator. Each phoswich is wrapped with white teflon tape and then surrounded with an aluminum foil. All the PMT's are surrounded by a cylindrical μ-metal shield (not shown in figs. 1 and 2 for clarity).

This configuration allows the detection of protons from 6.3 MeV up to 200 MeV. The energy threshold to identify an ^{16}O ion is 12.8 MeV/nucleon, 20.1 MeV/nucleon for a ^{40}Ca (Z = 20) ion and 23.2 MeV/nucleon for a ^{86}Kr (Z = 36) ion. These values are suitable since the first INDRA ring is mainly responsible for the detection of the fast projectile-like component which, at the GANIL energies, lies in most cases above these threshold values.

3. Electronics and the treatment of signals

Specific electronics was developed for the CsI(Tl) detectors of INDRA [14]. This electronics was modified and adapted for the phoswich detectors [15].

3.1. Design of the electronics (cf. fig. 3)

The information pertaining to the energy deposited in the thin (ΔE) and thick (E) scintillators has to be retrieved from the unique signal i(t) delivered by the PMT anode. Unfolding of this signal into its two constitutive components i) the fast one $i_F(t)$ related to the thin fast scintillator, ii) the slow one $i_S(t)$ related to the thick slow scintillator, has to be done with the best selectivity to allow a clear separation of the two signals i.e. a good identification of the fragments detected in the final instance. After the signal has been split into two channels :

$$i_1(t) = \alpha\, i(t), \qquad i_2(t) = (1-\alpha)\, i(t) \tag{1}$$

Unfolding is obtained by integrating over two time periods, a short one $T_1 - T_0$ and a longer one $T_2 - T_0$. The resulting signals :

$$V_1(t) = k_1 \int_{T_0}^{T_1} i_1(t)dt = k_1 \int_{T_0}^{T_1} \alpha\, i(t)\, dt\,, \quad V_2(t) = k_2 \int_{T_0}^{T_2 > T_1} i_2(t)dt = k_2 \int_{T_0}^{T_2 > T_1} (1-\alpha)\, i(t)dt \tag{2}$$

carry the wanted information : $\Delta E = f_1(V_1)$ corresponding to the energy deposited in the fast scintillator and $E = f_2(V_2)$ the energy in the slow scintillator. Ideally, one would have $\Delta E = a_1V_1$; $E = a_2V_2$. Practically, linearity is impaired i) by the physical processes involved in the conversion of energy to light into the scintillators, ii) by saturation effects into the PMT and associated circuits. A wise choice of the scintillating material and of its thickness helps to improve point i) for a given range of deposited energies as discussed previously. A careful choice of the PMT itself and of the design of its associated circuitry has allowed us to minimize the incidence of point ii). To maintain these qualities, a particular care has been taken into the design of the integrators and associated circuits. This care was first exercised through the determination of the parameters α, k_1, k_2, T_1, T_2 in the integrators. Then, every effort has been made to maintain the stability of each parameter, as this quality determines, with the minimization of noise sources, the resolution of the system. These aims were attained through the following steps :

a) Use of a passive splitter (cf. ① in fig. 3) to generate the currents $i_1(t)$ and $i_2(t)$ from the anode current i(t). This ensures good stability associated with a large dynamical range and the simplicity to modify the splitting parameter α, if necessary. Experimental tests with different ions and energies led us to adopt $\alpha = 5/6$.

b) A constant fraction discriminator ② [14] to ensure an accurate positionning of the gate signals for the integrators and provide a reliable discrimination against the noise plus a large dynamical range.

c) Specifically designed integrators ③ , ④ for accurate determination of the charges in the fast and slow channels [14, 15]. Integration is provided by charging a capacitor with a current proportionnal to i_1 or i_2. A pedestal current ensures good linearity and special measures have been put in use to ensure reliable discharging of the integration capacitor. This avoids memory effects on consecutive events. When charged to V_1 (V_2) , this capacitor acts as an analog memory to allow time for the event selection electronics to process the logic signals and decide on the subsequent digital conversions of V_1 (V_2). The parameters k_1 and k_2 depend on the values chosen for the integrating capacitors C_1 and C_2. Their values were determined after on-beam tests with consideration of the maximum current reliably delivered by the PMT's and the acceptable dynamic range of the circuits. This led to $C_1 = 250$ pF, $C_2 = 150$ pF then $Q_1 = 1.87$ nC, $Q_2 = 1.12$ nC, where Q_1 and Q_2 are the maximum charges resulting from the integrations. This part of the circuit was built from discrete components in a first version, which provided us with optimization and verification of the design. A later version has been realized using an Application Specific Integrated Circuit (ASIC) [16].

d) The gate generators ⑤ [14] deserve special attention as they assume an important role in the separation of the fast and slow components of the signal. This happens through the precise placement on the time scale of the parameters T_0, T_1, T_2 in eq. (2). The values retained for the gate widths are $T_1 - T_0 = 30$ ns ; $T_2 - T_0 = 800$ ns. Furthermore, a validation gate is

generated, which plays a role in the selection of valid events under the control of the general trigger circuit of INDRA [13]. To allow for accurate placement of the gates and reliable determination of their duration, the technique of generating step waveforms from linear ramps plus amplitude comparators, was retained. This permits flexible control of the parameters over a wide range of time scales.

Finally, a test generator ⑥ was devised and included into each of the 16 channels to allow remote checking of the circuits and periodic measurement of the pedestals in the integrators. The generator delivers particle-like signals to the input of the circuit under concern to simulate normal operation. Amplitude of the test signals is remote controlled.

3.2. Operation of the circuits and generation of data

Every channel that receives a signal of sufficient amplitude to cross its discriminator threshold triggers its own gate generators and integrates the received signal. The resulting voltages V_1 and V_2 are held on the integrating capacitors that act as analog memories.

After the integration is completed the channel circuit waits for a validation gate (FT), sent by the main trigger. This validation gate is compared with a signal generated by the discriminator of every channel that has been delayed by a fixed time (1μs). If this comparison results in a coincidence, then the channel is validated and the digital conversion of V_1 and V_2 is initiated. The resulting voltages are multiplexed towards an ADC. Otherwise, the channel is inhibited and its integrators are reset (cf. fig. 3).

This type of operation avoids using costly cables to delay the analog signals (this applies to all channels of INDRA) which would normally be necessary with the usual mode of operation. Its implicit limitation is that it is feasible only with a low rate of events, namely, one that gives not less than a few times the dead time of one channel (2 μs typically). Encoding of the twelve channels and transfer of data are implemented as in fig. 4.

3.3. Implementation of the circuits

Sixteen identical channels have been integrated on a D-size VXI module [15] using surface mount technology with multi-layered printed-circuit boards. The analog circuitry for each channel is implemented in discrete components mounted on a plug-in subcard that can be changed easily. These modules, like all the front-end electronics of INDRA, are located in close proximity to the detector, that is, in the same room as the reaction chamber. The use of VXI/VME technology permits the choice of remote commands and controls. This allows the operation, calibration and monitoring of all the electronics to be done on-line from the acquisition room [13].

Use of VXI/VME instrumentation on INDRA also allows to pass a variety of commands to the front-end electronics [13]. As regards the phoswiches, the following commands are implemented : i) threshold of the input discriminators ; ii) time delays (R, R+D) for timing the discriminators output signals, (CFD) ; iii) duration of the fast and slow integrating gates, (FFR, DFL, FFL) and iv) time of scrutation for the logic signals used for the validation of a channel (PV) (cf. fig. 3).

Besides these commands, a number of control signals can be routed to the control room via dedicated logic and analog bus-wires. These bus-wires can be connected to check-points on every channel by multiplexing on command to allow, for example, on-line display of the gate signals (to check their position and duration relative to the analog input signal).

Overall testing of the detector and associated circuits is done on command by injection of light pulses into the back of every phoswich at a rate of 10 pulses per second. The light pulses are generated by excitation of a piece of NE102 scintillator with light impulses from a nitrogen laser, then conveyed to each phoswich by optical fibers [1]. Moreover, as indicated in the previous section, a test generator is included into every channel of the electronics (fig. 3). This generator is activated, at will, from the console in the control room, via the VXI/VME commands. The charge injected can be controlled in the same way. This permits to check operation of the complete electronics of each channel, and ensure of the validity of response of the integrators.

The accessibility of all these commands and controls from the control room permits to monitor the behaviour of the critical points of the detector and to take the required means of correction or change parameters at every instant. This gives the complete detector great flexibility and the user a comprehensive mastery of its operation.

4. Heavy ion identification

4.1. Two-dimensional spectra

Figs. 5 and 6 show two dimensional spectra of the fast signal Q_F versus the total signal Q_T. Fig. 5 presents data from the Ar + Ni reactions cumulated over the whole beam energy range available at GANIL for Ar projectiles : elements up to the beam atomic number are very well separated over a fairly large domain, ranging from threshold (18 MeV/nucleon for Ar) up to 95 MeV/nucleon. Fig. 6 displays data measured in the $^{86}Kr + ^{27}Al$ reaction at 60 MeV/nucleon. A good charge resolution is observed up to $Z = 37$. In these figures, the data points are confined in a region approximately bounded by two lines : one line sloping away from the vertical axis and another one rising above the horizontal axis. The former line is made up of charged products which are stopped in the fast plastic scintillator. In this case, there

is no component from the slow scintillator, only the fast component is integrated in both fast and total gates ($Q_F = p_1.Q_T$). The latter line, stretching beyond the fast Z = 1 particle line is due to the detection of gammas, neutrons and cosmic rays in the slow plastic scintillator, as it constitutes the main part of the detector material. In that case, only a slow component is integrated in the two gates ($Q_F = p_2.Q_T$, with $p_2 \ll p_1$).

Contrary to the usual ΔE-E map, in which the ΔE signal decreases with the increase of the E signal, in case of plastic phoswiches, we deal with ΔL-L maps, with a ΔL or Q_F signal being the integration of two components, the fast one and the slow one, over a short time. Since the slow component increases with the energy and that a fraction of it is integrated during the fast gate, we observe an increase of the Q_F signal with the energy.

4.2. Particle identification

Thin fast plastic scintillators are needed to identify heavy ions with moderate energy thresholds. However, the resolution of the identification is inversely proportional to the thickness of the fast scintillators, due to fluctuations of light production and collection. As a result, the elemental Z lines are very close to each other (see, for example, fig. 5), and the Z identification cannot be performed satisfactorily using appropriate masks on the two dimensional maps Q_F - Q_T. Moreover, such a procedure is very unsuitable when applied to large Z values.

In the case of a large number of detectors, and as far as only light particles and nuclei are concerned, a superimposition of several Q_F-Q_T maps can be performed [5,9], thus reducing significantly the number of masks to be drawn. When dealing with heavier nuclei and thinner scintillators, a gain matching of the Q_F-Q_T plots from individual detectors is no longer possible. Thus, we chose a linearization procedure using the following parameterization [17] :

$$Q_F = \frac{a_1}{Q_T - a_2} + a_3 + a_4 Q_T \qquad (3)$$

which has been found to provide the best fit to the data. We did not try to derive such an equation from the energy-range relationship or from any relation between the amount of light and the energy. The only concern was the best description of the experimental Z lines as explained below.

The main advantage of the linearization procedure is to obtain a unique function describing all the Z lines at once, $Q_F = f(Q_T, Z)$, in such a way that the atomic number Z is deduced from the following equation :

$$Q_F^{exp} - f(Q_T^{exp}, Z) = 0 \qquad (4)$$

in which Q_F^{exp} and Q_T^{exp} are respectively the fast and total signals of a fragment with atomic number Z and energy E.

For this purpose, a three step method is followed. First, the two dimensional maps Q_F - Q_T are scanned in an automatic way in order to extract the coordinates of the ridges of each ion species [18]. Then, these coordinates (Q_F^i, Q_T^i, Z_i) are fitted with the function defined in eq. 3, in which a Z dependence has been introduced via the a_i coefficients, defined as :

$$a_i = \sum_{j=1}^{n} \alpha_{ij} Z^{j-1} \qquad (5)$$

Finally, the experimental Z-value is extracted from eq. 4 either analytically or by numerical resolution. Indeed, the degree of the polynomial is closely linked to the behaviour of the data. In case of a few lines and of a narrow energy domain, n = 2 or 3 values adjust the data in a satisfactory way and lead to simple analytical solutions of eq. 4. On the other hand, when faced with a great number of atomic species and a large energy range, the specific curvatures of every Z lines, especially that of the Z =1 and 2 particles, require a higher degree of the polynomial and, consequently, numerical calculations should be applied in order to solve eq. 4.

In table 1 are listed the α_{ij} coefficients of the identification function deduced from the data shown in fig. 5. In fig. 7 is displayed the charge distribution of fragments measured in the reaction Kr + Al at 60 MeV/nucleon (see fig. 6). As seen, an unambiguous separation of all charges is achieved up to Z = 37. This shows that the identification method described above is very powerful in getting the atomic numbers of ion species even if not well separated, as seen in the two dimensional spectrum in fig. 6. On the whole spectrum of fig. 7, the charge resolution is 0.7 charge unit (FWHM).

5. Energy calibration

As it is well known [19], the light output of plastic scintillators shows a non linear dependence with the energy deposited and depends on both the charge and the mass of fragments [20]. The absolute energy calibration of phoswich detectors needs different particle species with well defined charges, masses and energies, over a large range both in charge and energy. As already done elsewhere [5, 8, 9], fragmentation beams have been used to obtain calibration points. The particles were produced in the stopping of primary ^{16}O and ^{36}Ar beams in a thick carbon target, then they were selected by a magnetic spectrometer and scatterred on a thin gold target in the reaction chamber of INDRA. With such a technique, we obtained a variety of species ranging from hydrogen up to argon at several energies, corresponding to different magnetic rigidities. The measurement of the elastic scattering of the secondary particles and fragments prevents from dismounting the detectors. All the phoswich detectors are calibrated at once, as well as other detectors of INDRA (Si detectors and CsI(Tl) scintillators) located at small angles [1].

A fairly simple expression [5] commonly used to fit the data is the following :

$$E = F(Z)\,(L - L_0)^{\gamma} \qquad (6)$$

where E is the energy, L the total light output, L_0 the offset of the light output resulting from the pedestal in the ADC converters, γ a constant close to unity and F(Z) a function which introduces a dependence on the ion charge.

Several empirical functions F(Z) were used. The best fit to the data was obtained with the following expression :

$$E = F_1(Z)\,(L - L_0)^{\gamma} + F_2(Z) \qquad (7)$$

with $F_1(Z)$ and $F_2(Z)$ given by :

$$F_i(Z) = C_{1i}\,Z^{C_{2i}} + C_{3i} + \frac{C_{4i}}{C_{5i}Z^{C_{6i}} - C_{7i}} \qquad (8)$$

Since the total signal Q_T corresponds to the whole energy deposited in the phoswhich, it was used for the energy calibration. For each calibration point, corresponding to a fragment with given A, Z and E, the channel number corresponding to the total light produced in both scintillators was determined. This channel value was given an energy value in MeV, taking into account the elastic scattering between 2° and 3° as well as the energy loss in the target.

With the fragmentation beam technique, a lot of isotopes is produced allowing an energy calibration of the phoswiches depending on both the charge and the mass of fragments. However, as seen in the previous section, the limited resolution prevents from reaching an isotopic identification. Therefore, a mass dependence has not been introduced in the parameterization. For each phoswich detector, more than 300 points were fitted with the expression given in eq. 7. Coefficients obtained for one detector are given in table 2. Values of the γ constant (cf. eq. 6) have been found to lie between 0.82 and 0.93. Typical χ^2 / ν values of 1.2 were obtained in the fitting procedure. The results of such a procedure are illustrated in fig. 8. The full lines have been calculated using eq. 7 and coefficients of table 2. As shown, the parameterization covers a very large energy domain ranging from 10 MeV for Z = 1 up to 6.5 GeV for Z = 54 (calibration points obtained with Xe beams are not displayed in fig. 8). Of special interest, is the fact that the simple parameterization of eq. 7 offers a very satisfactory calibration on large dynamic ranges in energy and Z at once and the same time. Typical energy resolutions of ~ 4 - 5 % for light ions and ~ 10 % for heavier ions are reached (FWHM).

6. Conclusion

We have used phoswich detectors in the context of a 4π multidetector and we succeeded in the extension of their performance in element separation up to Z = 37, using thicknesses of 500 μm for the fast NE102 plastic scintillator and 25 cm for the slow NE115 plastic scintillator. In addition to the large dynamic mass covered, such a device allows working on a very large energy range, from 10 MeV protons up to 6.5 GeV Xe ions. In spite of the high thresholds, these detectors are well suited for event rebuilding in the forward direction. A new method of identification has been developed which is able to resolve elements up to Z ~ 40. Calibration of the detectors has been obtained via a unique parameterization on a large dynamic range in energy and atomic number. These improvements of the phoswich technique lead to a full agreement with the requirements and specificities of the INDRA multidetector.

Acknowledgements :

We wish to thank B. Chambon, D. Horn, C. Pastor, J. Pouliot and R. Roy for many helpful discussions and A. Genoux-Lubain and J.P. Patry for assistance during the experiments. We are indebted to the Service d'Electronique Physique from IPN Orsay for useful discussions and efficient cooperation. B. Berthier is greatly acknowledged for providing us with GEANT calculations. We thank also the staffs of the SARA and GANIL machines for providing us with excellent quality beams.

REFERENCES

[1] J. Pouthas, B. Borderie, R. Dayras, E. Plagnol, M.F. Rivet, F. Saint-Laurent, J.C. Steckmeyer, G. Auger, C.O. Bacri, S. Barbey, A. Barbier, A. Benkirane, J. Benlliure, B. Berthier, E. Bougamont, P. Bourgault, P. Box, R. Bzyl, B. Cahan, Y. Cassagnou, D. Charlet, J.L. Charvet, A. Chbihi, T. Clerc, N. Copinet, D. Cussol, M. Engrand, J.M. Gautier, Y. Huguet, O. Jouniaux, J.L. Laville, P. Le Botlan, A. Leconte, R. Legrain, P. Lelong, M. Le Guay, L. Martina, C. Mazur, P. Mosrin, L.Olivier, J.P. Passerieux, S. Pierre, B. Piquet, E. Plaige, E.C. Pollacco, B. Raine, A. Richard, J. Ropert, C. Spitaels, L. Stab, D. Sznajderman, L. Tassan-Got, J. Tillier, M. Tripon, P. Vallerand, C. Volant, P. Volkov, J.P. Wieleczko and G. Wittwer ; GANIL P 9426, submitted to Nucl. Inst. and Meth.

[2] Nuclear Enterprises Technology Ltd ; Edinburgh, F G11 4BY Scotland.

[3] K. M. Teh, D. Shapira, B. L. Burks, R. L. Varner, J. L. Blankenship, E. J. Ludwig, R. E. Fauber and C. F. Maguire ; Nucl. Instr. and Meth. A254 (1987) 600

[4] F. Lidén, A. Johnson, A. Kerek, E. Dafni and M. Sidi ; Nucl. Instr. and Meth. A273 (1988) 240

[5] J. Pouliot , Y. Chan, A. Dacal, A. Harmon, R. Knop, M. E. Ortiz, E. Plagnol and R.G. Stokstad ; Nucl. Instr. and Meth. A270 (1988) 69

[6] M. M. Fowler, T. C. Sangster, M. L. Begemann-Blaich, T. Blaich, J. A. Boissevain, H. C. Britt, Y. D. Chan, A. Dacal, D. J. Fields, Z. Fraenkel, A. Gavron, A. Harmon, B. V. Jacak, R. G. Lanier, P. S. Lysaght, G. Mamane, D. J. Massoletti, M.N.Namboodiri, J. Pouliot, R. G. Stokstad, M. L. Webb and J. B. Wilhelmy ; Nucl. Instr. and Meth. A2181 (1989) 517

[7] C. A. Pruneau, G. C. Ball, P. Dmytrenko, E. Hagberg, D. Horn, C. Rioux, R. Roy, C. Saint-Pierre, T. E. Dracke and A. Galindo-Uribarri ; Nucl. Instr. and Meth. (1990)

[8] H.K.W. Leegte, E. E. Koldenhof, A. L. Boonstra and H. W. Wilschut ; Nucl. Instr. and Meth. A313 (1992) 26.

[9] D.A. Cebra, W. K. Wilson, A. Vander Molen and G. D. Westfall ; Nucl. Instr. and Meth. A313 (1992) 367

[10] E. Migneco, C. Agodi, R. Alba, G. Bellia, R. Coniglione, A. Del Zoppo, P. Finocchiaro, C. Maiolino, P. Piattelli, G. Raia and P. Sapienza ; Nucl. Instr. and Meth. A314 (1992) 31.

[11] J.B. Costales, H.C. Britt, M.N. Namboodiri, T.C. Sangster, J.H. Thomas and H.E. Wegner ; Nucl. Instr. and Meth. A330 (1993) 183

[12] R. Brun, F. Bruyant, M. Maire, A.C. Mc Pherson and P. Zanarini ; CERN report DD/EE/84-1

[13] J. Pouthas et al ; in preparation
P. Volkov, private communication

[14] J.C. Artiges, D. Charlet, J. Deschamps, A. Richard and J. Clément, Conf. Records of 1991 IEEE - NSS, Santa Fé, 1991, p. 728
A. Richard et al ; Proc. of Int. Conf. on New Nuclear Physics with Advanced Techniques, Ierapetra, Greece, june 23-29, 1991

[15] A. Leconte ; thesis, CNAM, LPCC T 94-03, Caen, unpublished

[16] Bouvier, H. Bugnet, D. Dzahimi, R. Foglio, J. Pouxe and M. Tournier ; Proceedings of the IEEE Nuclear Science Symposium and Medical Imaging Conference, 1993, p. 547

[17] J.C. Steckmeyer ; internal report, LPCC 91-05, Caen, unpublished

[18] A. Benkirane, G. Auger, D. Bloyet, A. Chbihi and E. Plagnol ; GANIL P 9420 and Nucl. Instr. and Meth. (in press)
O. Grand ; internal report, ISMRA, Caen, 1992, unpublished

[19] J.B. Birks ; The Theory and Practice of Scintillation Counting, Pergamon Press, Oxford, 1964

[20] M.A. Mc Mahan ; IEEE Trans. Nucl. Sci. NS-35 (1988) 42.

FIGURE CAPTIONS

Fig. 1 : Split view of the INDRA multidetector. The phoswich ring is seen on the most right part of the figure. The cylindrical μ-metal shield is not shown.

Fig. 2 : Schematic of the phoswich ring of INDRA. All the PMT's are surrounded by a cylindrical μ-metal shield, not shown in the figure for clarity.

(A) Side view from back

(B) Front view as seen by the beam.

Fig. 3 : Schematic diagram of one analog channel.

Fig. 4 : Schematic diagram of encoding and data transfer.

Fig. 5 : A two-dimensional histogram of the fast signal Q_F versus the slow signal Q_T . This plot is a summing-up of Ar + Ni data at 40, 52, 63, 74, 84 and 95 MeV/nucleon. The full curves represent the identification function defined in eqs. 3 and 5 with the α_{ij} coefficients as listed in table 1.

Fig. 6 : A two-dimensional histogram of the fast signal Q_F versus the slow signal Q_T measured in Kr + Al interactions at 60 MeV/nucleon.

Fig. 7 : Charge distribution of fragments recorded at $2° \leq \theta \leq 3°$ in the reaction Kr + Al at 60 MeV/nucleon as displayed in fig. 6.

Fig. 8 : Absolute energy calibration of the total signal of a phoswich detector of the forward ring of INDRA. Symbols correspond to different ion species as labelled in the figure (odd atomic numbers in the left part, even atomic numbers in the right one). Not shown in the figure some calibration points obtained with Xe beams.

α_{ij}	i = 1	i = 2	i = 3	i = 4
j = 1	.43487 E + 00	.99907 E + 01	.70749 E + 04	-.14711E + 03
j = 2	.41306 E - 02	.22918 E + 02	.69001 E + 03	-.14990E + 02
j = 3	.41039 E - 07	.16328 E - 05	.35697 E - 01	.96034 E + 00
j = 4	.69047 E - 08	-.85383 E - 01	.39046 E - 02	.14052 E - 01
j = 5	.18304 E - 09	.24898 E - 02	.53375 E + 01	.11971 E - 02

Table 1 : Coefficients of the identification function of a phoswich detector (see eqs. 3 and 5) This identification function is displayed in fig. 5 as full lines.

C_{ji}	i = 1	i = 2
j = 1	.433031 E + 02	-.616124 E + 04
j = 2	.218167 E - 01	.163789 E - 01
j = 3	-.424688 E + 02	.564379 E + 04
j = 4	-.712814 E - 01	.119222 E + 04
j = 5	.762048 E + 03	.301973 E + 03
j = 6	.249833 E - 02	-.159432 E - 02
j = 7	.762352 E + 03	.299727 E + 03

Table 2 : Coefficients of the calibration function of a phoswich detector (see eqs. 7 and 8). This calibration function is displayed in fig. 8 as full lines.

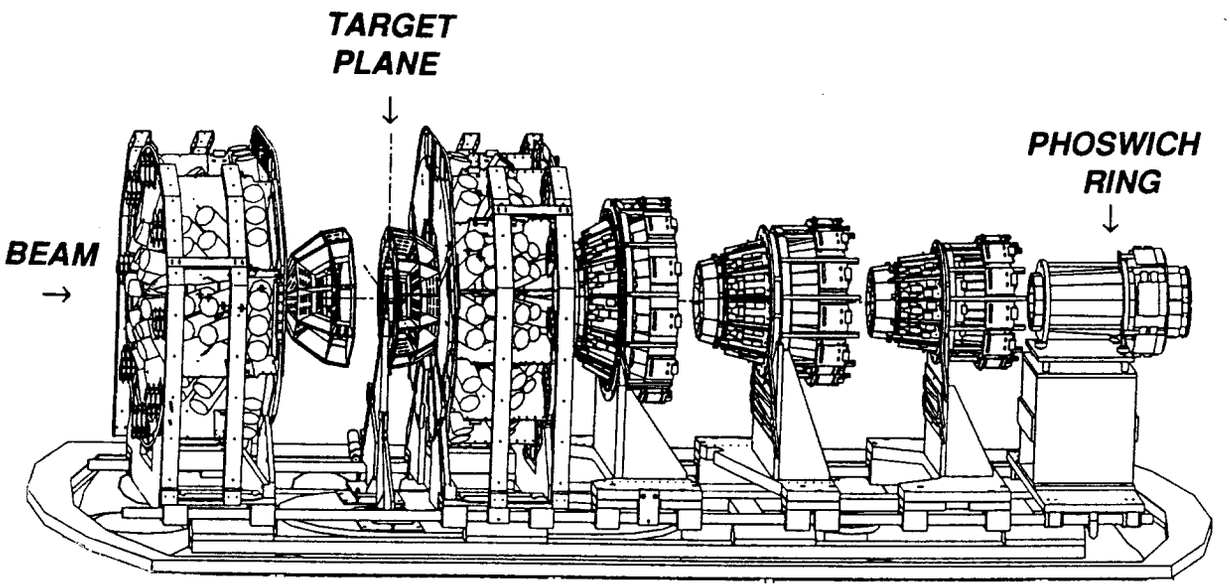

Figure 1

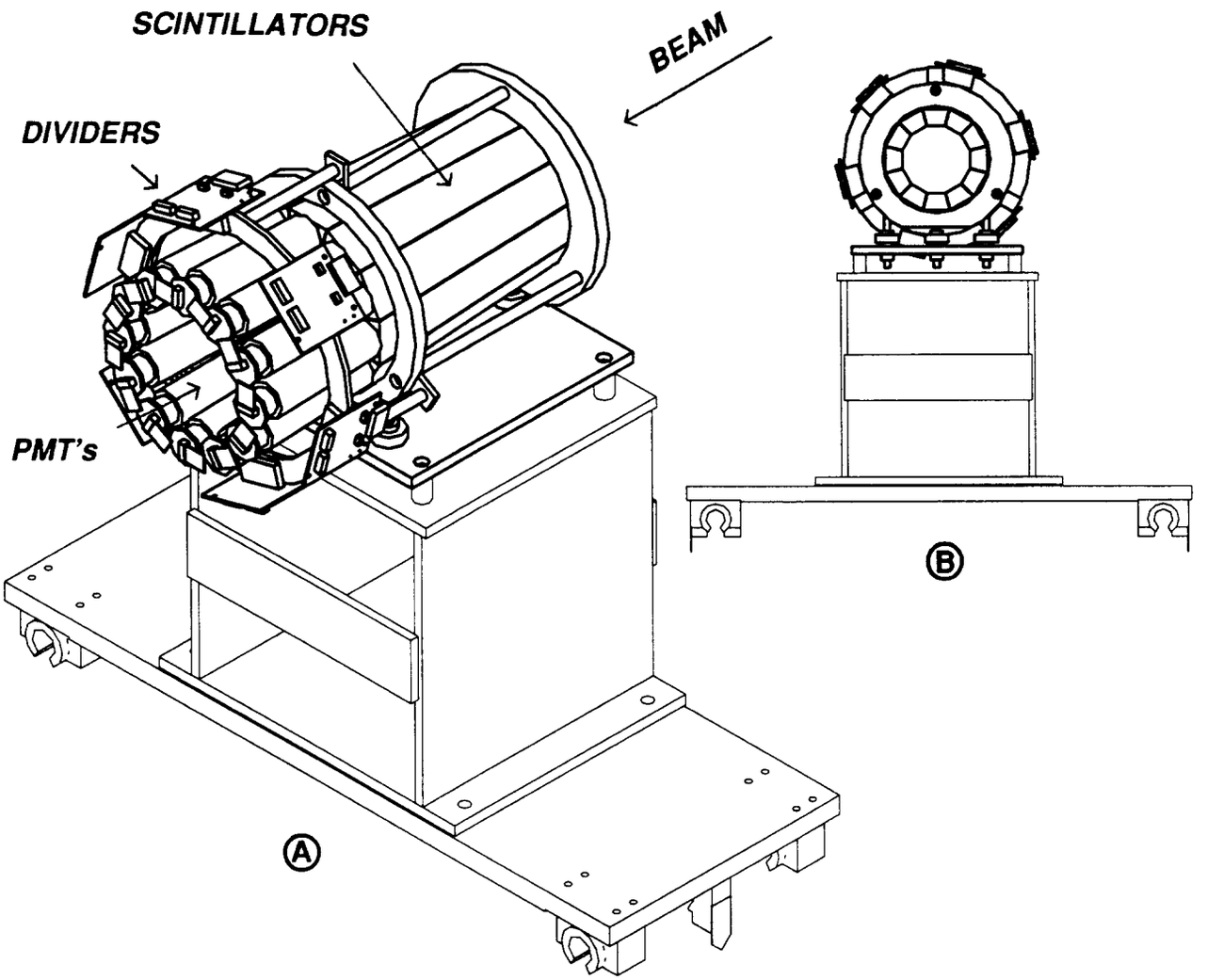

Figure 2

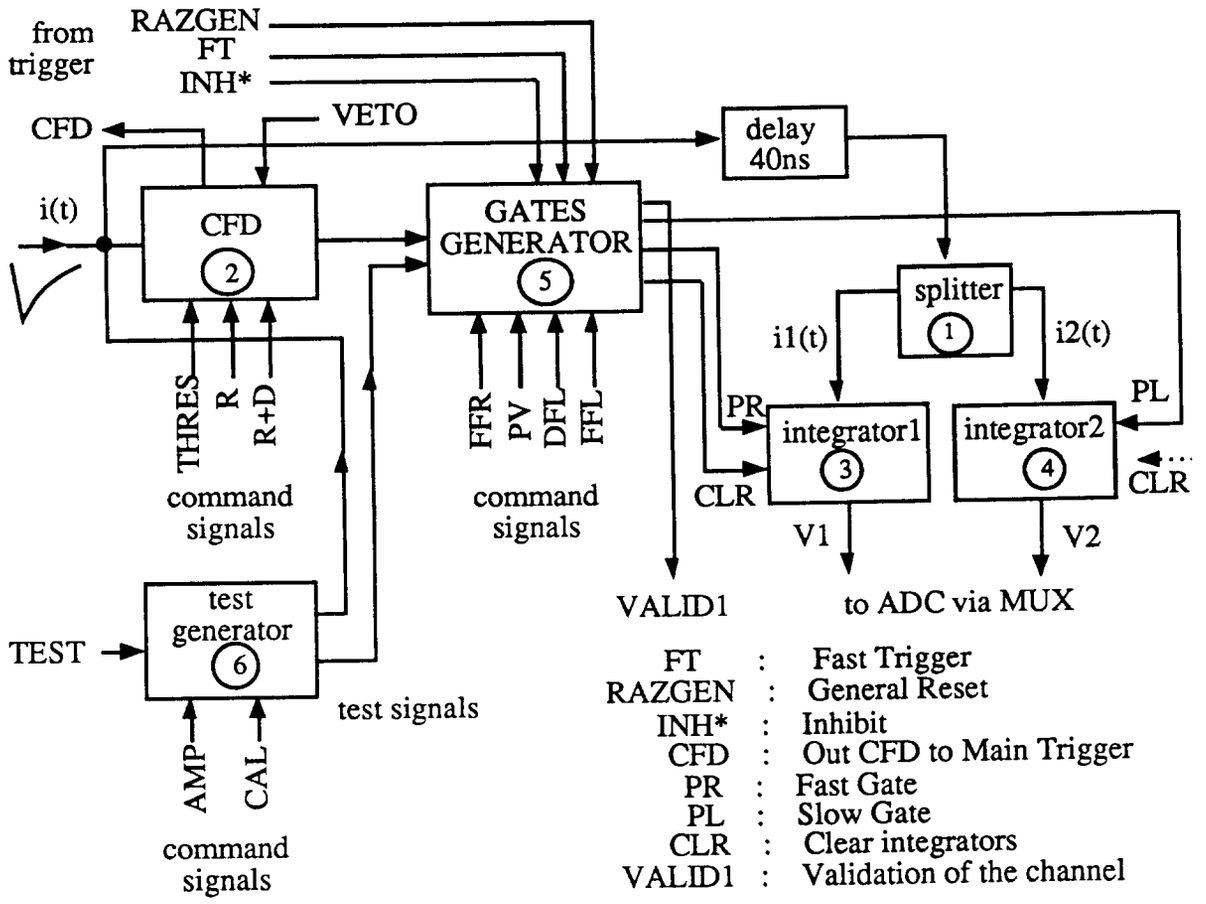
from trigger
RAZGEN
FT
INH*
VETO
CFD
delay 40ns
i(t)
CFD
2
GATES GENERATOR
5
splitter
1
i1(t)
i2(t)
PR
PL
integrator1
3
integrator2
4
CLR
CLR
THRES
R
R+D
command signals
FFR
PV
DFL
FFL
command signals
V1
V2
VALID1
to ADC via MUX
test generator
6
TEST
test signals
AMP
CAL
command signals
FT : Fast Trigger
RAZGEN : General Reset
INH* : Inhibit
CFD : Out CFD to Main Trigger
PR : Fast Gate
PL : Slow Gate
CLR : Clear integrators
VALID1 : Validation of the channel

Figure 3

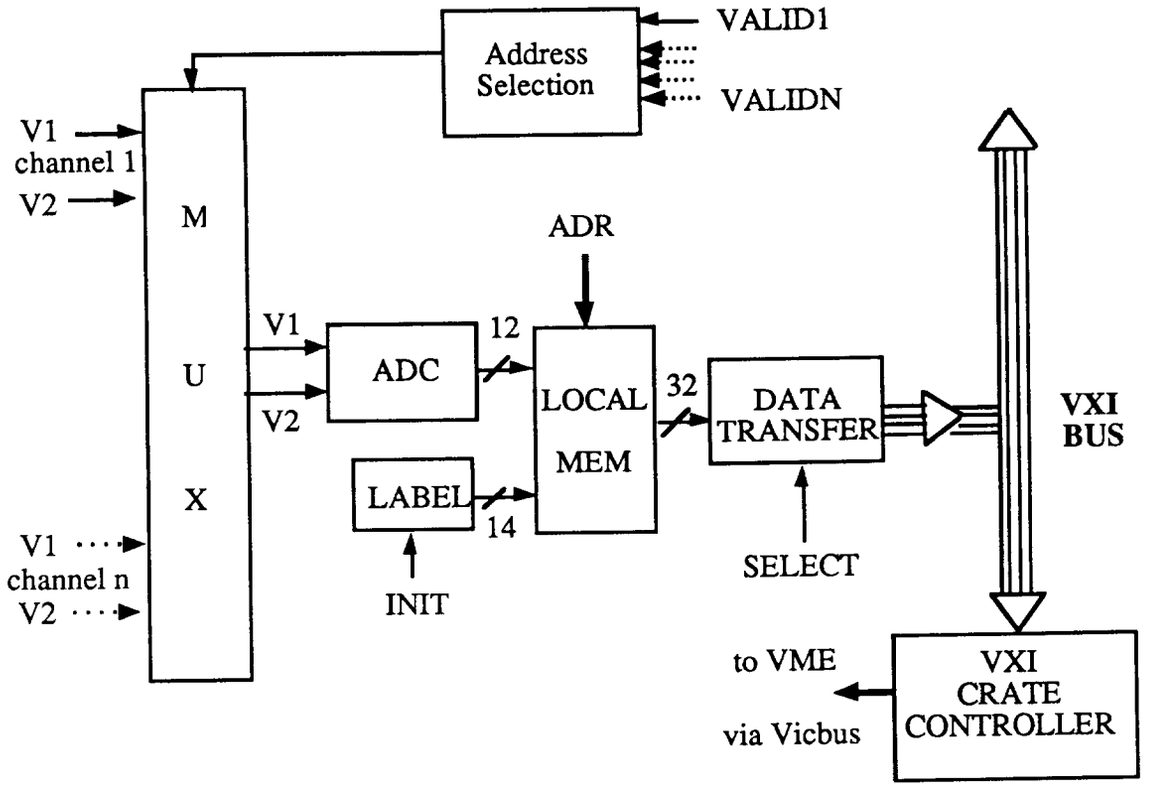
Address
Selection
VALID1
VALIDN
V1
channel 1
V2
M
U
X
V1
channel n
V2
V1
V2
ADC
12
ADR
LOCAL
MEM
32
DATA
TRANSFER
VXI
BUS
LABEL
14
INIT
SELECT
to VME
via Vicbus
VXI
CRATE
CONTROLLER

Figure 4

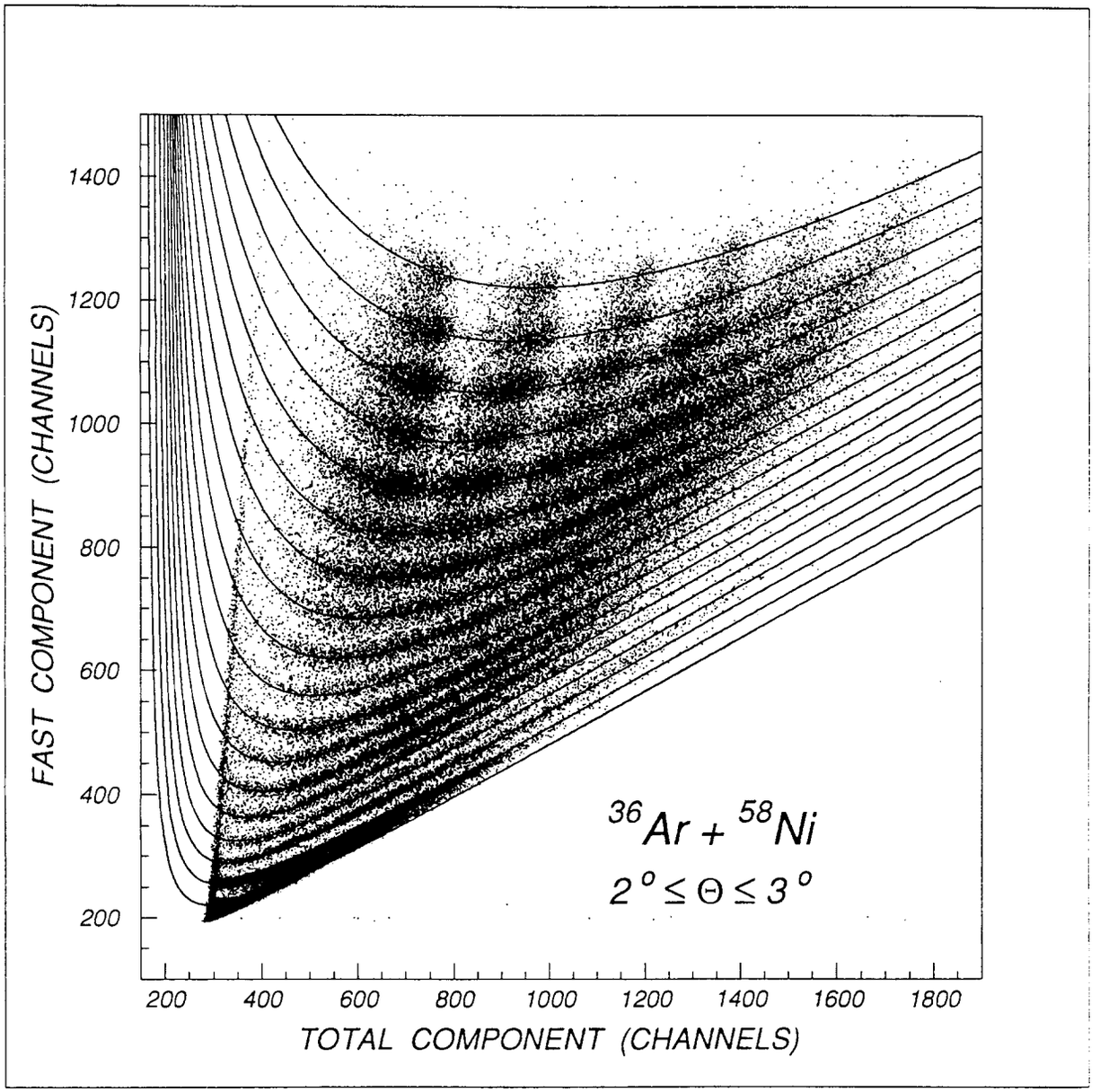
FAST COMPONENT (CHANNELS)
1400
1200
1000
800
600
400
200
200
400
600
800
1000
1200
1400
1600
1800
TOTAL COMPONENT (CHANNELS)
$^{36}Ar + ^{58}Ni$
$2^{o} \leq \Theta \leq 3^{o}$

Figure 5

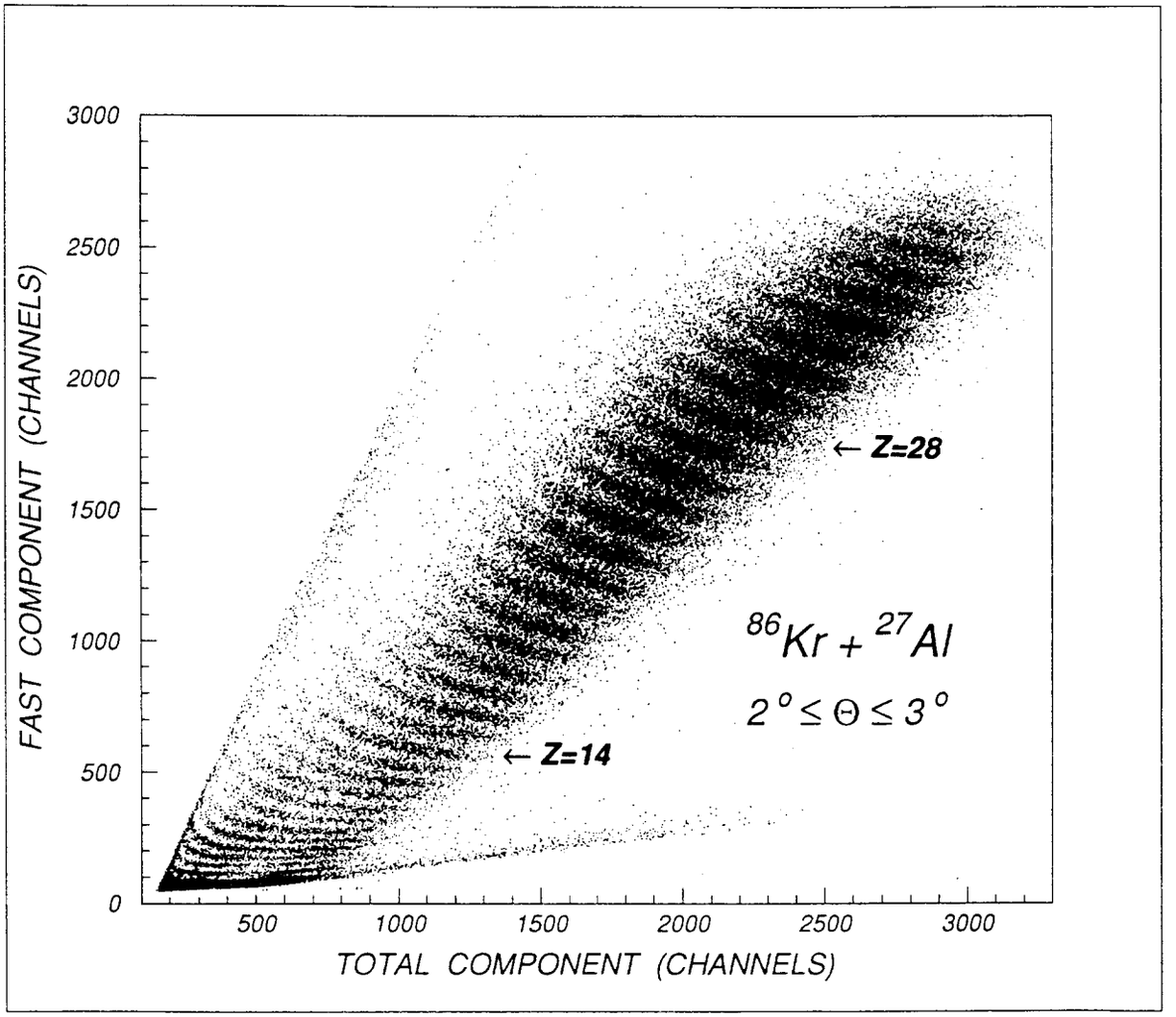
3000
2500
2000
1500
1000
500
0
FAST COMPONENT (CHANNELS)
500
1000
1500
2000
2500
3000
TOTAL COMPONENT (CHANNELS)
← Z=28
← Z=14
86Kr + 27Al
2° ≤ Θ ≤ 3°

Figure 6

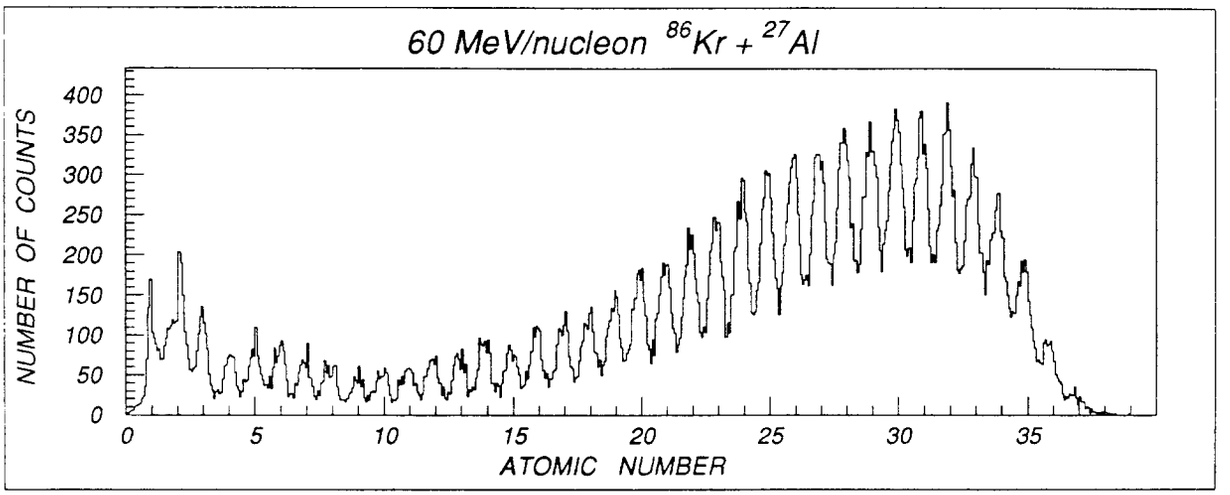
60 MeV/nucleon $^{86}Kr + ^{27}Al$
NUMBER OF COUNTS
400
350
300
250
200
150
100
50
0
0
5
10
15
20
25
30
35
ATOMIC NUMBER

Figure 7

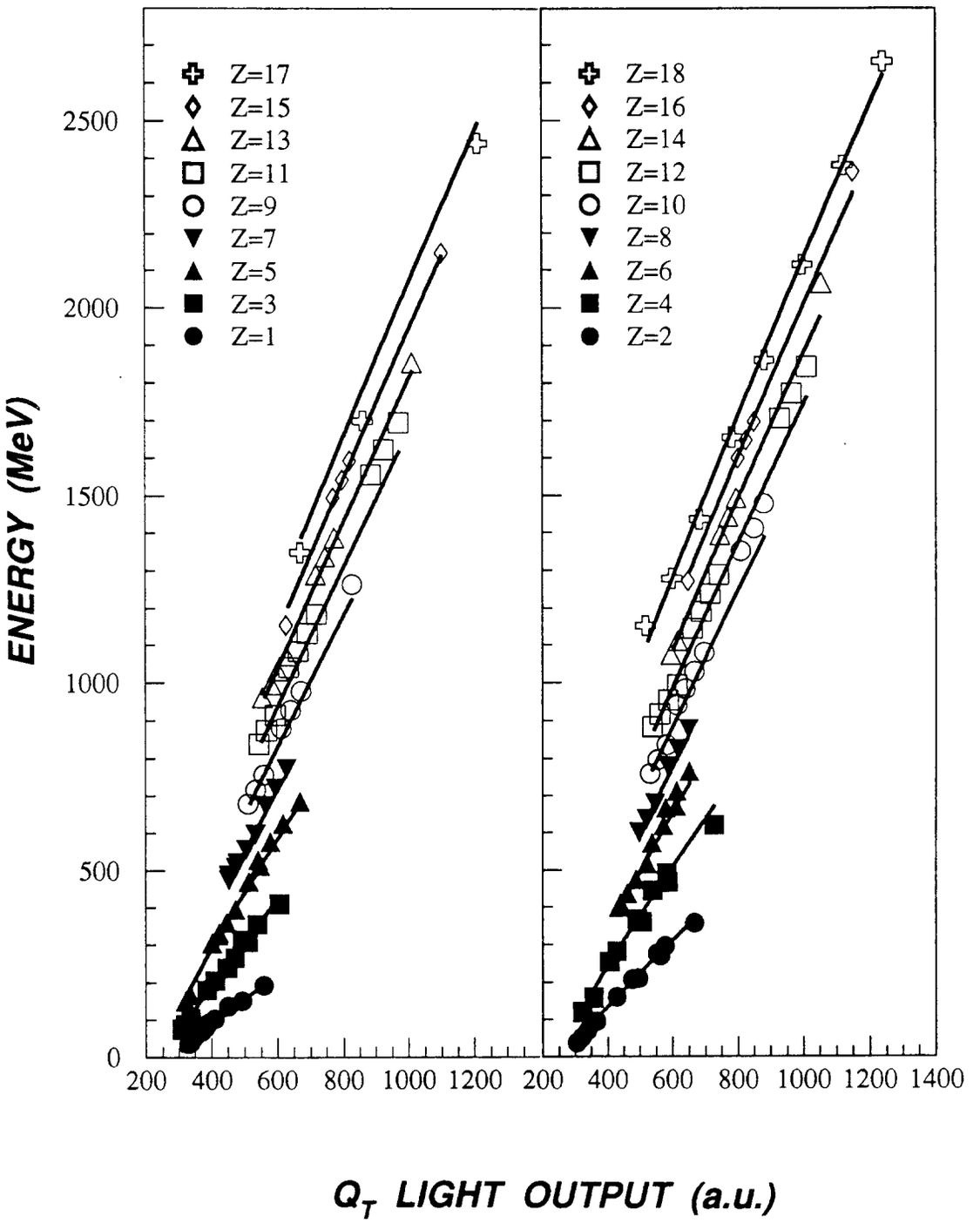
Z=17
Z=15
Z=13
Z=11
Z=9
Z=7
Z=5
Z=3
Z=1
Z=18
Z=16
Z=14
Z=12
Z=10
Z=8
Z=6
Z=4
Z=2
ENERGY (MeV)
0
500
1000
1500
2000
2500
200
400
600
800
1000
1200
1400
Q_T LIGHT OUTPUT (a.u.)

Figure 8